Title Page

Contribution of cellular contractility to spatial and temporal variations in cellular stiffness

Masafumi Nagayama[1,*], Hisashi Haga[2], Masayuki Takahashi[3], Takayuki Saitoh[2] and Kazushige Kawabata[2]

Division of [1]Physics, [2]Biological Sciences, [3]Chemistry, Graduate School of Science, Hokkaido University, Sapporo 060-0810, Japan

[*]Corresponding author. Current address: Department of Applied Physics, Graduate School of Engineering, Hokkaido University, North 13, West 8, Kita-ku, Sapporo 060-8628, Japan.

Tel/Fax: +81-11-706-6637

E-mail address: macci@eng.hokudai.ac.jp (M. Nagayama).

Abstract

Scanning probe microscopy and immunofluorescence observations indicated that cellular stiffness was attributed to a contractile network structure consisting of stress fibers. We measured temporal variations in cellular stiffness when cellular contractility was regulated by dosing with lysophosphatidic acid or Y-27632. This experiment reveals a clear relation between cellular stiffness and contractility: Increases in contractility cause cells to stiffen. On the other hand, decreases in contractility reduce cellular stiffness. In both cases, not only the stiffness of the stress fibers but also that of the whole of the cell varies. Immunofluorescence observations of myosin II and vinculin indicated that the stiffness variations induced by the regulation of cellular contractility were mainly due to rearrangements of the contractile actin network on the dorsal surface. Taken together, our findings provide evidence that the actin cytoskeletal network and its contractility features provide and modulate the mechanical stability of adherent cells.

Keywords: Fibroblast, Scanning probe microscopy, Atomic force microscopy, Lysophosphatidic acid, Y-27632, Stress fiber, Actomyosin, Mechanical stability

Introduction

Cellular functions such as migration, proliferation, differentiation, and apoptosis play a critical role in various biological and pathological phenomena at the tissue level, including the healing of wounded tissue, the self-organization of early embryos, the immune response, and the metastasis of tumor cells. The mechanisms regulating cellular function have thus been widely investigated in various disciplines. For example, it has previously been demonstrated that the Rho family of small GTPases including Rho, Rac, and Cdc42 is a key regulator of cytoskeletal dynamics, which are essential for achieving coordinated and directed cellular migration [1-3]. When specific receptors on the cellular surface bind to growth factors or to extracellular matrix (ECM), these small GTPases are activated by guanine nucleotide exchange factors (GEFs) [4]. In molecular biology and biochemistry, some of the signaling pathways that induce the reorganization of the cytoskeleton by the active GTPases have been identified [5]. Such signaling pathways account for how subcellular migrations such as lamellipodia extension, tail retraction, cell body contraction, and turnover of focal contacts occur. On the other hand, it was revealed that the cell adhering to a substratum exerted contractile forces, and that the forces exhibited a macroscopic pattern dependent on cellular polarity [6]. It has thus been suggested that anisotropic contractile forces provide a directional traction force required for cellular migration. The spatial distribution of the traction force that a single cell exerts has been obtained quantitatively by using flexible gel [7] or microneedle substratum [8]. Temporal variations in the traction force exerted during cellular migration have also been reported [9,10]. However, when subcellular migrations occur independently, cells cannot produce such a directed traction force. Each subcellular process must be spatially and temporally coordinated at the cellular level; this

requirement applies not only to cellular migration, but to other cellular functions as well.

Understanding cellular functions as an integrated phenomenon requires not only studies of the chemical properties of molecules and proteins, but also macroscopic studies of the mechanical properties of the multicomponent structures comprising these molecules [11]. The mechanical properties of the cellular cortex have been measured by several techniques such as cell poking [12,13], micropipette aspiration [14,15], optical tweezers [16-18] and magnetic beads twisting [19-21]. However, the temporal and/or spatial resolutions of these techniques do not suffice for a thorough understanding of the variations in mechanical properties caused by cellular functions.

Scanning probe microscope (SPM) has rapidly developed as a powerful tool for obtaining a topographic image of biological samples with high resolution (scale: nanometer) in their natural aqueous environment. SPM can also be used to evaluate mechanical properties, because its probe is in physical contact with the samples during measurement. To obtain cellular stiffness with SPM, two methods have been proposed, namely, a force modulation mode [22,23] and a force mapping mode [24]. According to experiments performed by using these methods, the local stiffness of fibroblasts is not homogeneous on the cellular surface, but varies largely from point to point [25,26]. Immunofluorescence observations indicate that the spatial distribution of stiffness can be primarily attributed to filamentous actin (F-actin) rather than to microtubules and intermediate filaments of cytoskeleton [27]. This attribution is also supported by other experiments showing that the disruption of F-actin by treatment with cytochalasinB drastically reduces cellular stiffness [28,29]. A previous experiment by our group revealed a clear relation between cellular migration and the distribution of local stiffness on fibroblasts [30]: When cells are stationary, the distribution of stiffness on the cellular surface is quite stable. On the other hand, once the cells start to migrate, the stiffness in their nuclear regions drastically decreases. F-actin forms a contractile bundle through association with

myosin II, and this bundle is referred to as a stress fiber. The contractile force generated by stress fibers can drag the cell body forward during cellular migration. Thus, the temporal variation in stiffness during cellular migration can be thought to be due to the variation in contractile force.

In the present study, we revealed a contribution of contractile actin network to the spatial distribution of local stiffness of a fibroblast. Then, we measured temporal variations in cellular stiffness when cellular contractility was regulated by dosing with two types of biochemical reagent. The following two advantages led us to perform the stiffness imaging with SPM. One advantage of SPM is that the response of a single cell to dosing with reagents can be assessed. The other advantage is that the relation between cellular stiffness and contractility can be assessed without the formation of adhesions between the probe and the cell surface. We also observed the spatial distribution of myosin II and vinculin after cellular contractility was regulated. These experiments suggested that the contractile actin cytoskeleton acts as a mechanical network that covers the entire cell and modulates the mechanical stability of the adherent cell.

Materials and Methods

Cell culture and sample preparation

Due to the following experimental requirements, fibroblasts (NIH3T3) derived from mouse embryos were used for the present experiments: (i) as the cells were exposed to scanning with a probe during SPM imaging, they had to adhere strongly to the substratum; and (ii) studies of the migration of single cell required that the cell had high motility and did not form cell-cell contacts.

The fibroblasts were purchased from the RIKEN Cell Bank (Tsukuba, Japan) and were grown

in plastic flasks filled with culture medium. The medium consisted of low-glucose Dulbecco's modified Eagle's medium (DMEM) supplemented with 10% fetal bovine serum (FBS) (Gibco BRL, Basel, Switzerland). A suitable amount of antibiotics was also added to the DMEM (Gibco BRL, Basel, Switzerland). The plastic flasks were maintained at 37˚C and 5% CO_2 in a humidified incubator during the cell culture period. For the present experiments, confluent fibroblasts were tripsinized and then released from the flask. The cell suspension was plated on a glass petri dish (diameter, 30 mm; height, 3 mm) precoated with fibronectin (Boehringer Mannheim, Mannheim, Germany). Fibroblasts plated on each dish were incubated again for at least one night in order to ensure firm adherence.

To maintain the pH constant at 7.3 during SPM measurements performed in an environment of open air, preheated HEPES-buffer was substituted for the culture medium at least 1 hour before the measurements were carried out.

SPM imaging of living cells

The commercial instrument used in this study consisted of an SPA400 equipped with a piezo scanner with a maximum *x-y* range of 100×100 μm and a *z* range of 10 μm, and an SPI3800 control unit (Seiko Instruments Inc., Chiba, Japan). When the spring constant of the cantilevers is equivalent to that of the cells, the highest sensitivity for measuring viscoelasticity is achieved. We used a commercially available silicon-nitride cantilever, which was a triangle with an effective length of 320 μm (ThermoMicroscopes, Sunnyvale, CA). A pyramidal tip, the typical radius of curvature of which is about 50 nm, is placed on one end of the cantilever. According to the calibration by the thermal fluctuation method, the spring constant of the cantilevers was 7.5 mN/m. During the measurements, a petri dish filled with HEPES-buffer must be kept at physiological temperature. The

dish was placed on a metal plate maintained at 33±0.5˚C by a temperature controller that consisted of a heater and a thermocouple. To prevent rapid evaporation of the buffer, the temperature had to be set approximately 5˚C lower than that of the cell culture. Under these conditions, each fibroblast adhered firmly and extended thinly on the dish for over 3 hours, even after the SPM measurements. These findings verified that physiological conditions were maintained during the present experiments and that the scanning probe over the cellular surface did not cause any damage to the fibroblasts.

Force mapping mode

The force mapping mode with SPM is generally used to measure the Young's modulus of soft materials such as cells and gels [27,31]. In this mode, a force-versus-distance curve (force curve) was taken while a cantilever was indenting into each point on the surface of the sample. By using nonlinear least squares fitting (NLSF), the force curve taken at one point of sample surface was fitted to Sneddon's model, a theoretical model in which the elastic contact theory of Hertz is applied to contact between an elastic plane and a rigid cone (the details are described in Ref. [32]). This fitting allowed to evaluate not only the Young's modulus but also the *z*-position, where the cantilever initially contacts the sample (i.e., the height of the sample at the point). In the present study, the force curve was fitted in the loading force range of 0.1-0.3 nN. The cellular Poisson ratio was assumed to be 0.5. Under the condition that a single force curve was taken for 100 milliseconds, each image consisting of 64×64 pixels was able to obtain in approximately 40 minutes. We confirmed that the experimental force curve was well reproduced by the fit curve (data not shown).

Generally, Young's modulus is defined as a value expressing the elastic properties of a homogenous elastic or viscoelastic body. However, cells consist of heterogeneous structures.

Moreover, the mechanical response from the cellular surface was expected to be the result of a large number of mechanical effects, including osmotic pressure and the mechanical properties of the cell membranes and the cytoskeleton. In the present study, the obtained Young's modulus was thus regarded as not an elastic modulus but an effective value of local stiffness.

Fluorescence imaging

For the immunofluorescence observation, the fibroblasts were washed once with PBS and were fixed with 4% formaldehyde/PBS for 10 minutes, and then were washed again with PBS. After fixation, the fibroblasts were permeabilized with 0.5% Triton X-100/PBS for 10 minutes and were washed twice with PBS, and then were incubated with PBS containing 0.5% bovine serum albumin (BSA) for 40 minutes. The permeabilized fibroblasts were incubated with primary antibodies/PBS containing 0.5% BSA for 1 hour and were rinsed with PBS containing 0.5% BSA three times. Then, the fibroblasts were incubated with secondary antibodies/PBS containing 0.5% BSA for 1 hour and were rinsed three additional times.

Anti-myosin heavy chain-IIA (MHC-IIA) polyclonal antibody was produced against a synthetic peptide, D-E-E-V-D-G-K-A-D-G-A-E (i.e., the carboxyl-terminus of human nonmuscle MHC-IIA). Immunization and purification of the antibody were performed according to a published protocol [33]. The antibody to MHC-IIB has been described previously [34]. Myosin IIA and IIB were detected with 0.2% anti-MHC-IIA and with 0.2% anti-MHC-IIB, respectively, as a primary antibody. Both of the myosin II isoforms recognized with the primary antibodies were stained with 0.4% Alexa Fluor 488-labeled anti-rabbit IgG (Molecular Probes, Inc., Eugene, OR) as a secondary antibody. F-actin was labeled with 1.0% Alexa Fluor 546-phalloidin (Molecular Probes, Inc., Eugene, OR). Vinculin, a known protein localized at focal contacts, was detected with 0.5% anti-human

vinculin (Sigma-Aldrich, St. Louis, MO) as the primary antibody, and 0.3% Cy3-labeled anti-mouse IgG (Jackson ImmunoResearch Lab. Inc., West Grove, PA) as the secondary antibody.

Fluorescence imaging was performed using a confocal laser scanning microscope (CLSM) equipped with an 100× oil immersion objective (PCM2000, NIKON, Tokyo, Japan). In the present experiment, an Ar laser (wavelength λ = 488 nm) and an He-Ne laser (λ = 543.5 nm) were used as excitation lights. Sectional fluorescence images were captured at intervals of 0.3 μm, ranging from the bottom to the top of a cell.

Biochemical reagents

In the present study, we treated the fibroblasts with either lysophosphatidic acid (LPA) or Y-27632, in order to regulate the cellular contractility. The phosphorylation of the myosin regulatory light chain (RLC) is essential for the formation of stress fibers originating from the interactions between myosin II and F-actin. It is known that the phosphorylation of RLC is complementarily regulated by two signaling pathways that involve (i) myosin light chain kinase (MLCK) and (ii) myosin light chain phosphatase (MLCP) [35-37]. LPA activates small GTPase RhoA via G-protein coupled receptors and GEFs. Then, Rho kinase (ROK) is activated by the active RhoA, and subsequently inhibits the phosphatase activity of MLCP. Consequently, LPA increases cellular contractility. The fibroblasts were stimulated by dosing them with 5 μM LPA (Sigma-Aldrich, St. Louis, MO). On the other hand, treatment with Y-27632, a known inhibitor of ROK, reduces cellular contractility. The fibroblasts were treated by the administration of 10 or 20 μM Y-27632 (Calbiochem, San Diego, CA).

Each petri dish on which the fibroblasts were plated was filled with DMEM without FBS, and then was incubated for one night before the experiments were carried out. The reason for using

DMEM without FBS was that the exclusion of soluble growth factor enhanced the effect of dosing with the reagents on the actin-myosin II interactions. Under the present conditions, the fibroblasts extended thinly on the surface of each glass dish due to pretreatment of the dish with a fibronectin coating.

Results

Contribution of the cytoskeletal network consisting of F-actin and myosin II to the spatial distribution of stiffness

Figs. 1A and B show topographic and stiffness images of a living fibroblast, respectively. In the topographic image (Fig. 1A), the cell extended thinly (height, approximately 2.5 μm; lateral length, over 80 μm) on the substratum. The highest region in the topography represents the cell nucleus. Here, the fibroblast was highly polarized in three directions. In the stiffness image (Fig. 1B), the values of Young's modulus ranged from a few kPa to 40 kPa over the cellular surface. Many stiff fibers ran in parallel with the cell polarity. A stiff domain (arrowhead, Fig. 1B) was located in the vicinity of the nucleus, but the surface area just above the nucleus was softer than that of the surrounding area (circle, Fig. 1B). Immunofluorescence staining of the identical cell was performed just after the SPM experiment, and then the fluorescence images were captured using CLSM. The distribution of F-actin and myosin II containing two isoforms on the dorsal surface is shown in Figs. 1C and D, respectively. Each image was reconstructed from a series of sectional images, with the exception of that of the ventral surface. Although many filamentous structures can be seen in both images, these structures were found to be clearly different in terms of the following characteristics:

the fibers shown in Fig. 1C were very clearly observed as solid lines, whereas those in Fig. 1D appeared like dashed lines, i.e., like lines consisting of numerous dots. Fig. 1E shows an image in which those of Figs. 1C and D are merged. In the merged image, the yellow area represents the region where F-actin and myosin are colocalized. The stiff fibers shown in Fig. 1B corresponded well to the colocalized fibers shown in Fig. 1E (i.e., the stress fibers). This finding suggested that cellular stiffness originates not in a rigid, but rather in a contractile framework consisting of F-actin associated with myosin II. The stiff domain corresponded to the site at which the stress fibers converged (i.e., the area designated by the arrowhead in Fig. 1B should be compared with that in Fig. 1E). Two other stiff domains that appeared on the surface near the cell nucleus (arrows, Fig. 1B) also corresponded to the site at which several stress fibers converged into a thick bundle (arrows, Fig. 1E). In other words, the stiff domains included stress fibers that branched in two or more directions. Although myosin II did not form a clear filamentous structure, it was highly concentrated in all stiff domains (arrowhead and arrows, Fig. 1D). The same correspondence of cellular stiffness to the distribution of F-actin and myosin II was observed in two other cells without exception.

Effects of the cellular contractility on the stiffness

To examine the relationship between cellular stiffness and contractility, stiffness images were obtained when contractility was regulated by treatment with biochemical reagents. Fig. 2 shows a temporal variation in the topographic and stiffness images of a fibroblast stimulated with 5 μM LPA, which served to increase cellular contractility [35-37]. The topographic images (Figs. 2A and B) were captured before and at 30 minutes after stimulation, respectively. Before stimulation, the fibroblast extended thinly on the substratum. For the 30 minutes after stimulation by LPA, the height of the fibroblast decreased to approximately 0.5 μm lower than it was before the treatment with LPA.

Figs. 2C and D show the respective stiffness images that corresponded to the topographic images (Figs. 2A and B). Before stimulation, stiff fibers originating in the stress fibers appeared on the cellular surface. The cellular surface above the nucleus was softer than its surroundings. Stimulation by LPA increased the stiffness of the stress fibers (arrowhead, Figs. 2C and D). Although the cellular surface above the nucleus was softer than its surroundings, the stiffness of this region also increased after stimulation (arrow, Figs. 2C and D). Figs. 2E and F illustrate some of the stiff structures extracted from the stiffness images (Figs. 2C and D). The stimulation by LPA created new stiff domains that appeared on the cellular surface near the nucleus. The drastic increase in cellular stiffness due to stimulation by LPA was not consistently observed in all of the experiments. In eight experiments, the four fibroblasts became stiffer, but the other four fibroblasts neither changed nor reduced their stiffness.

Contrary to the effects of LPA, treatment with Y-27632 reduced cellular contractility [35-37]. Fig. 3 shows temporal variation in the topographic and stiffness images of a fibroblast after treatment with 20 μM Y-27632. The topographic images (Figs. 3A and B) were captured before and at 20 minutes after treatment, respectively. The fibroblasts treated with Y-27632 seemed to slightly shrink. However, numerous small lamellipodia appeared on the edge of the cells after the treatment (arrows, Fig. 3B). The height of the fibroblast was approximately 0.3 μm higher than before the treatment with Y-27632. A round shape representative of the cell nucleus appeared clearly on the surface. Figs. 3C and D are the stiffness images that correspond to the respective topographic images (Figs. 3A and B). Before treatment, many stress fibers clearly appeared on the cellular surface (arrowhead, Fig. 3C). The treatment with Y-27632 reduced the stiffness not only of the stress fibers (arrowhead, Fig. 3D) but also of the entire cell. The softer region corresponding to the cell nucleus appeared to expand. Figs. 3E and F illustrate some of the stiff structures extracted from the stiffness

images (Figs. 3C and D). Although several stress fibers still remained, treatment with Y-27632 led to the disappearance of two stiff domains (arrows, Fig. 3E). Similar results were observed in all of the experimental cells, without exception (n=4).

Effects of the regulation of cellular contractility on the rearrangement of the contractile cytoskeleton

To clarify the origins of the variations in stiffness induced by the regulation of cellular contractility (Figs. 2 and 3), we observed the rearrangement of the contractile cytoskeleton network after cellular contractility was regulated. Figs. 4A and B show the spatial distribution of myosin II on the dorsal and ventral surfaces of a cell, respectively, at 30 minutes after stimulation by 5 μM LPA. In Fig. 4A, many myosin II fibers, representing stress fibers, ran in parallel across the entire cell. The domains in which myosin II was highly concentrated appeared in the vicinity of the nucleus (arrows, Fig. 4A). These domains were thought to correspond with the stiff domains shown in the SPM results (arrows, Fig. 1D). On the ventral surface, densely arranged stress fibers were present in the central region of the cell (Fig. 4B). Fig. 4C shows the spatial distribution of myosin II (*green*) and vinculin (*red*); this image contain both distributions of myosin II and vinculin on the dorsal as well as the ventral surface of the cell. It was found that each stress fiber terminated at focal contacts. Taking the information presented in Figs. 4A and B into consideration, this merged image indicated that the stress fibers could be distinguished by the following characteristics: on the dorsal surface, long stress fibers extended to the periphery of the cell, and terminated at the focal contacts there at the periphery (arrows, Fig. 4C). On the other hand, stress fibers running along the ventral surface were shorter than those running along the dorsal surface, and the ventral fibers did not reach the periphery (arrowhead, Fig. 4C).

We also captured immunofluorescence images of myosin II and vinculin in a cell at 30 minutes after treatment with 10 μM Y-27632. Figs. 4D and E show the spatial distribution of myosin II on the dorsal and ventral surfaces of the cell, respectively. In contrast to the results observed with LPA (Figs. 4A and B), it was found that Y-27632 caused a decrease in the number of clear myosin II fibers (Figs. 4D and E). In this experiment, no highly concentrated domains of myosin II were observed, as is shown in Fig. 4D. Fig. 4F shows the spatial distribution of myosin II (*green*) and vinculin (*red*). These fluorescence images revealed that the treatment with Y-27632 had the following effects on the distribution of the stress fibers: Short stress fibers on the ventral surface still remained (arrowhead, Fig. 4F), whereas most of the long stress fibers disappeared on the dorsal surface.

These findings indicated that the regulation of cellular contractility leads to the rearrangement of the contractile cytoskeleton through the appearance and/or disappearance of stress fibers, especially on the dorsal surface. The relationship between cellular stiffness and contractility (Figs. 2 and 3) is expected to originate in such rearrangements of the contractile cytoskeleton.

Discussion

As shown in Fig. 1, each stress fiber appeared to radiate out in all directions from a single point of convergence (arrowhead, Fig. 1E). This finding suggested that all stress fibers might be connected to each other, thereby forming a contractile network that covers the entire cell. The contractile force that is integrated over the entire cell can be regarded as tension. We think that the coordination originating in tension plays an important role in the spatial distribution of stress fibers corresponding

with cellular polarity. This speculation is based on a simple simulation (Fig. 5). To demonstrate the spatial distribution of stress fibers, we introduced a two-dimensional meshwork made with elastic cords, as shown in Fig. 5A. The meshwork imitated the contractile network, which consists of stress fibers. The model was stretched and three points were pinned to the substratum by pushpins (Fig. 5B). The pushpins represented focal contacts. When tension was discretely supported by the pins, the mesh was distorted due to its own contractility. With respect to a radial pattern, the anisotropic pattern appearing in the mesh was in good agreement with that of F-actin (stress fibers) in an actual cell, as shown in Fig. 5C. The simulation demonstrated that anisotropic tension supported by discrete focal contacts could produce the spatial distribution of stress fibers. This concept is consistent with a tensegrity model known as a conceptual model of mechanical coordination between the parts of a cell and the cell as a whole [38-40].

A tense stress fiber would be stiffer than a relaxed stress fiber because the stiffness measured by SPM indicates the resistance (namely, *stability*) to deformation due to cantilever indentation. In the present study, Figs. 2 and 3 clearly show that the regulation of intracellular contractile forces induces variation in the stiffness of an entire cell. This finding means that the contractile network composed of stress fibers, which is discussed in detail above, provides for the mechanical stability of a cell; in addition, this network also modulates the mechanical stability. Thus, the contractile network functions much in the manner of a pillar or a roof for the formation and maintenance of 3-demensional shape of adherent cells.

Fig. 4 demonstrates that there is a close relationship between the regulation of cellular contractility and the rearrangement of the contractile cytoskeleton. It appears that such rearrangements of the contractile cytoskeleton can be caused by one or both of the two following mechanisms. The first mechanism is a biochemical process that is dependent on intracellular

signaling pathways that are initiated via transmembrane receptors and/or a stretched-activated calcium channel (SA channel) [41]. The other mechanism is a mechanical process that involves the deformation of the cytoskeleton network. The latter mechanism is illustrated in Fig. 5. Briefly, stress fibers in a cell can be arranged passively, whereby the arrangement depends entirely on tension and focal contacts. At this stage, it is difficult to determine which pathway is more dominant in the process of rearrangement. It is possible that both the biochemical and mechanical mechanisms interact with each other and thereby function as a positive feedback system.

In summary, we demonstrated in the present study the contribution of cellular contractility to spatial and temporal variations in cellular stiffness and the contractile cytoskeleton network. These findings provide evidence that the actin cytoskeletal network and its contractility modulate as well as create the mechanical stability of adherent cells. The modulation of mechanical stability may reflect a common mechanism regulating migration, proliferation, and self-organization at the tissue level; the present findings may provide useful information for the fields of cancer research and tissue engineering.

Acknowledgements

This work was supported in part by a Grant-in-Aid for JSPS Fellows to M.N., and by a Grant-in-Aid for Scientific Research from the Ministry of Education, Culture, Sports, Science and Technology of Japan to H.H. and K.K.

References

[1] F.N. van Leeuwen, S. van Delft, H.E. Kain, R.A. van der Kammen, J.G. Collard, Rac regulates phosphorylation of the myosin-II heavy chain, actinomyosin disassembly and cell spreading, Nat. Cell Biol. 1 (1999) 242-248.

[2] C.M. Waterman-Storer, E.D. Salmon, Positive feedback interactions between microtubule and actin dynamics during cell motility, Curr. Opin. Cell Biol. 11 (1999) 61-67.

[3] C.M. Waterman-Storer, R.A. Worthylake, B.P. Liu, K. Burridge, E.D. Salmon, Microtubule growth activates Rac1 to promote lamellipodial protrusion in fibroblasts, Nat. Cell Biol. 1 (1999) 45-50.

[4] M. Symons, J. Settleman, Rho family GTPases: more than simple switches, Trends Cell Biol. 10 (2000) 415-419.

[5] A.J. Ridley, Rho GTPases and cell migration, J. Cell Sci. 114 (2001) 2713-2722.

[6] A.K. Harris, P. Wild, D. Stopak, Silicone rubber substrata: a new wrinkle in the study of cell locomotion, Science 208 (1980) 177-180.

[7] M. Dembo, Y.-L. Wang, Stresses at the cell-to-substrate interface during locomotion of fibroblasts, Biophys. J. 76 (1999) 2307-2316.

[8] J.L. Tan, J. Tien, D.M. Pirone, D.S. Gray, K. Bhadriraju, C.S. Chen, Cells lying on a bed of microneedles: an approach to isolate mechanical force, Proc. Natl. Acad. Sci. USA. 100 (2003)

1484-1489.

[9] S. Munevar, Y.-L. Wang, M. Dembo, Traction force microscopy of migrating normal and H-ras transformed 3T3 fibroblasts, Biophys. J. 80 (2001) 1744-1757.

[10] S. Munevar, Y.-L. Wang, M. Dembo, Distinct roles of frontal and rear cell-substrate adhesions in fibroblast migration, Mol. Biol. Cell 12 (2001) 3947-3954.

[11] D.A. Lauffenburger, A.F. Horwitz, Cell migration: a physically integrated molecular process, Cell 84 (1996) 359-369.

[12] N.O. Peterson, W.B. McConnaughey, E.L. Elson, Dependence of locally measured cellular deformability on position on the cell, temperature, and cytochalasin B, Proc. Natl. Acad. Sci. USA 79 (1982) 5327-5331.

[13] G.I. Zaharak, W.B. McConnaughey, E.L. Elson, Determination of cellular mechanical properties by cell poking, with an application to leukocytes, J. Biomech. Eng. 112 (1990) 283-294.

[14] E. Evans, K. Ritchie, R. Merkel, Sensitive force technique to probe molecular adhesion and structural linkages at biological interfaces, Biophys. J. 68 (1995) 2580-2587.

[15] J.-Y. Shao, R.M. Hochmuth, Mechanical anchoring strength of L-selectin, beta2 integrins, and CD45 to neutrophil cytoskeleton and membrane, Biophys. J. 71 (1996) 2892-2901.

[16] A. Ashkin, J.M. Dziedzic, Internal cell manipulation using infrared laser traps, Proc. Natl. Acad. Sci. USA 86 (1989) 7914-7918.

[17] K. Svoboda, C.F. Schmidt, D. Branton, S.M. Block, Conformation and elasticity of the isolated red blood cell membrane skeleton, Biophys. J. 63 (1992) 784-793.

[18] S. Henon, G. Lenormand, A. Richert, F. Gallet, A new determination of the shear modulus of the human erythrocyte membrane using optical tweezers, Biophys. J. 76 (1999) 1145-1151.

[19] A.R. Bausch, F. Ziemann, A.A. Boulbitch, K. Jacobson, E. Sackmann, Local measurements of viscoelastic parameters of adherent cell surfaces by magnetic bead microrheometry, Biophys. J. 75 (1998) 2038-2049.

[20] A.R. Bausch, W. Moller, E. Sackmann, Measurement of local viscoelasticity and forces in living cells by magnetic tweezers, Biophys. J. 76 (1999) 573-579.

[21] N. Wang, D. Stamenovic, Contribution of intermediate filaments to cell stiffness, stiffening, and growth, Am. J. Physiol. Cell Physiol. 279 (2000) C188-C194.

[22] M. Radmacher, R.W. Tillmann, M. Fritz, H.E. Gaub, From molecules to cells: imaging soft samples with the atomic force microscope, Science 257 (1992) 1900-1905.

[23] M. Radmacher, R.W. Tillmann, H.E. Gaub, Imaging viscoelasticity by force modulation with atomic force microscope, Biophys. J. 64 (1993) 735-742.

[24] M. Radmacher, M. Fritz, C.M. Kacher, J.P. Cleveland, P.K. Hansma, Measuring the viscoelastic properties of human platelets with the atomic force microscope, Biophys. J. 70 (1996) 556-567.

[25] H. Haga, M. Nagayama, K. Kawabata, E. Ito, T. Ushiki, T. Sambongi, Time-lapse viscoelastic imaging of living fibroblasts using force modulation mode in AFM, J. Electron Microsc. 49 (2000)

473-481.

[26] M. Nagayama, H. Haga, Y. Tanaka, Y. Hirai, M. Kabuto, K. Kawabata, Improvement of force modulation mode with scanning probe microscopy for imaging viscoelasticity of living cells, Jpn. J. Appl. Phys. 41 (2002) 4952-4955.

[27] H. Haga, S. Sasaki, K. Kawabata, E. Ito, T. Ushiki, T. Sambongi, Elasticity mapping of living fibroblasts by AFM and immunofluorescence observation of the cytoskeleton, Ultramicroscopy 82 (2000) 253-258.

[28] C. Rotsch, M. Radmacher, Drug-induced changes of cytoskeletal structure and mechanics in fibroblasts: an atomic force microscopy study, Biophys. J. 78 (2000) 520-535.

[29] K. Kawabata, M. Nagayama, H. Haga, T. Sambongi, Mechanical effects on collective phenomena of biological systems: cell locomotion, Current Applied Physics 1 (2001) 66-71.

[30] M. Nagayama, H. Haga, K. Kawabata, Drastic change of local stiffness distribution correlating to cell migration in living fibroblasts, Cell Motil. Cytoskeleton 50 (2001) 173-179.

[31] T. Nitta, H. Haga, K. Kawabata, K. Abe, T. Sambongi, Comparing microscopic with macroscopic elastic properties of polymer gel, Ultramicroscopy 82 (2000) 223-226.

[32] A. Vinckier, G. Semenza, Measuring elasticity of biological materials by atomic force microscopy, FEBS Lett. 430 (1998) 12-16.

[33] M. Takahashi, T. Hirano, K. Uchida, A. Yamagishi, Developmentally regulated expression of a nonmuscle myosin heavy chain IIB inserted isoform in rat brain, Biochem. Biophys. Res. Commun.

259 (1999) 29-33.

[34] T. Saitoh, S. Takemura, K. Ueda, H. Hosoya, M. Nagayama, H. Haga, K. Kawabata, A. Yamagishi, M. Takahashi, Differential localization of non-muscle myosin II isoforms and phosphorylated regulatory light chains in human MRC-5 fibroblasts, FEBS Lett. 509 (2001) 365-369.

[35] M. Parizi, E.W. Howard, J.J. Tomasek, Regulation of LPA-promoted myofibroblast contraction: role of Rho, myosin light chain kinase, and myosin light chain phosphatase, Exp. Cell Res. 254 (2000) 210-220.

[36] A.P. Somlyo, A.V. Somlyo, Signal transduction by G-proteins, rho-kinase and protein phosphatase to smooth muscle and non-muscle myosin II, J. Physiol. 522 (2000) 177-185.

[37] J.T. Deng, J.E. Van Lierop, C. Sutherland, M.P. Walsh, Ca^{2+}-independent smooth muscle contraction. a novel function for integrin-linked kinase, J. Biol. Chem. 276 (2001) 16365-16373.

[38] D.E. Ingber, Tensegrity I. Cell structure and hierarchical systems biology, J. Cell Sci. 116 (2003) 1157-1173.

[39] D.E. Ingber, Tensegrity II. How structural networks influence cellular information processing networks, J. Cell Sci. 116 (2003) 1397-1408.

[40] S. Hu, J. Chen, B. Fabry, Y. Numaguchi, A. Gouldstone, D.E. Ingber, J.J. Fredberg, J.P. Butler, N. Wang, Intracellular stress tomography reveals stress focusing and structural anisotropy in cytoskeleton of living cells, Am. J. Physiol. Cell Physiol. 285 (2003) C1082-1090.

[41] G.T. Charras, M.A. Horton, Single cell mechanotransduction and its modulation analyzed by atomic force microscope indentation, Biophys. J. 82 (2002) 2970-2981.

Figure legends

Fig. 1.

Topographic (A) and stiffness images (B) of a living fibroblast were measured by the force mapping mode using SPM. Each image is an 80-μm square consisting of 64×64 pixels. The scale bar for stiffness is shown on a log scale (B). Many stiff fibers extend radially from a stiff domain (arrowhead, B). The corresponding structure with the fibers cannot be seen in the topographic image (A). The softer region (circle, B) corresponds to the position of the cell nucleus. The distribution of F-actin (C) and myosin II (D) on the dorsal surface of the identical cell were obtained using CLSM. Stiffer fibers and domains corresponded well with the areas in which myosin II was highly concentrated (arrowhead and arrows, B and D). In the merged image (E), red and green express F-actin and myosin II, respectively. The stiff domain was found to correspond to the site at which the stress fibers converged (arrowhead, E) or branched (arrows, E).

Fig. 2.

Temporal variations in cellular stiffness due to increases in contractility. Topographic (A) and stiffness images (C) of a living fibroblast were measured using the force mapping mode. At 30 minutes after stimulation by LPA, topographic (B) and stiffness images (D) of the identical fibroblast were measured again. The scale bar for stiffness is shown on a log scale (C, D). In the stiffness images, arrowheads and arrows indicate the regions above the stress fiber and the cell nucleus, respectively. Stimulation with LPA increased the stiffness not only of the stress fibers, but also of the entire cell. Schematic drawings (E, F) represent the distributions of stiff structures extracted from the

stiffness images (C, D), respectively. After stimulation, new stiff domains appeared on the surface near the cell nucleus.

Fig. 3.

Temporal variations in cellular stiffness due to reducing contractility. Topographic (A) and stiffness images (C) of a living fibroblast were measured using the force mapping mode. At 20 minutes after treatment with Y-27632, topographic (B) and stiffness images (D) of the identical fibroblast were measured again. The scale bar for stiffness is shown on a log scale (C, D). In the stiffness images, arrowheads indicate the stress fibers. Treatment with Y-27632 drastically reduced the stiffness of the entire cell. Schematic drawings (E, F) represent the distributions of stiff structures extracted from the stiffness images (C, D). Stiff domains in the vicinity of the cell nucleus (arrows, E) disappeared after the treatment.

Fig. 4.

Spatial distribution of myosin II and vinculin when cellular contractility was regulated. At 30 minutes after stimulation by 5 μM LPA (A-C) or after treatment with 10 μM Y-27632 (D-F), a series of sectional fluorescence images was captured by CLSM. The spatial distribution of myosin II on the dorsal surface (A, D) and on the ventral surface (B, E) was reconstructed from original sectional images. Superimposed images (C, F) of the distribution of myosin II (*green*) and vinculin (*red*) were also reconstructed; these images contain both distributions of myosin II and vinculin on the dorsal as well as the ventral surface. The contrasts of all images were linearly enhanced to make the images legible. Comparing each image (D-F) with the respective corresponding image (A-C), a reduction in contractility was found to lead to the rearrangement of the contractile cytoskeleton as follows. The

domains in which myosin II was highly concentrated (arrows, A) and the long stress fibers (arrows, C) disappeared on the dorsal surface. Short stress fibers (arrowheads, C and F) became unclear, but were still visible on the ventral surface.

Fig. 5.

A simulation reproducing the spatial distribution of stress fibers with the use of a simple model. A two-dimensional meshwork was created with elastic cords, which represented the contractile network structure (A). When the stretched mesh was pinned down at three points by pushpins, the mesh exhibited a radial pattern (B). The radial pattern was in good agreement with the typical pattern of stress fibers in an actual cell (C).

Figures

Fig. 1.

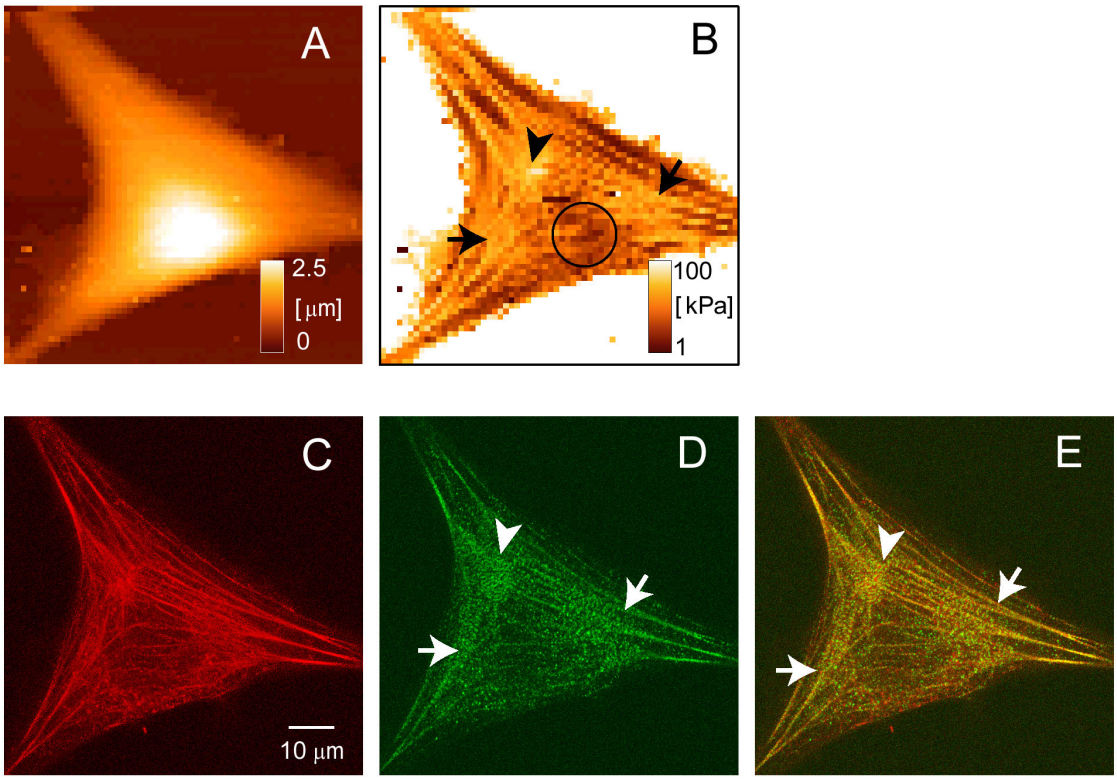

Fig. 2.

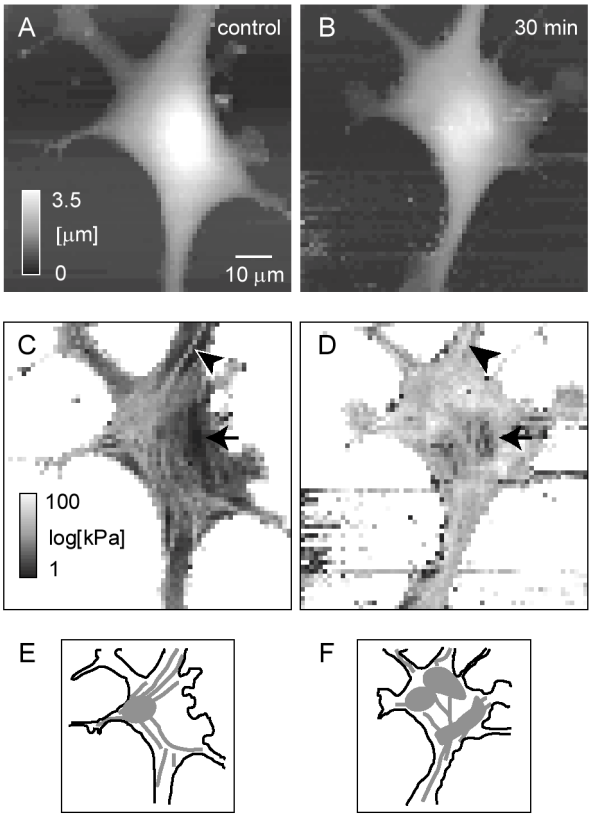

Fig. 3.

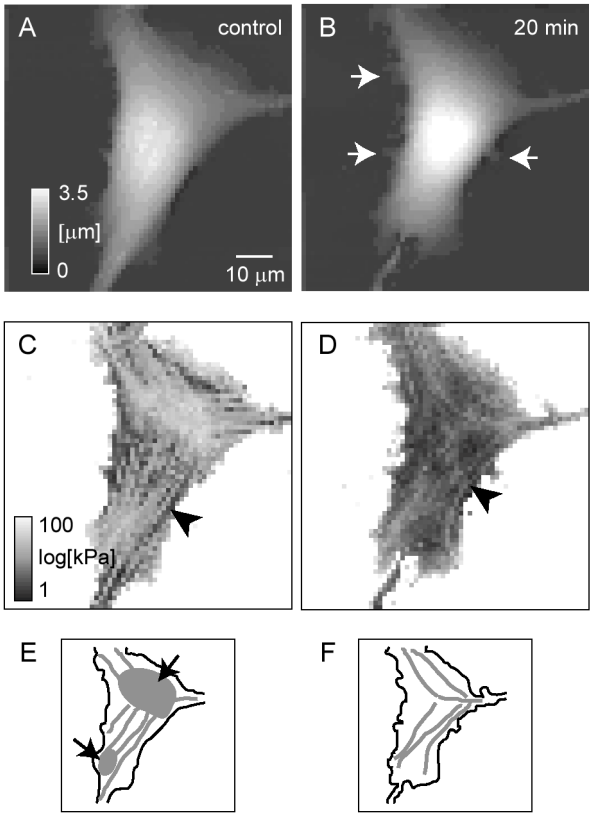

Fig. 4.

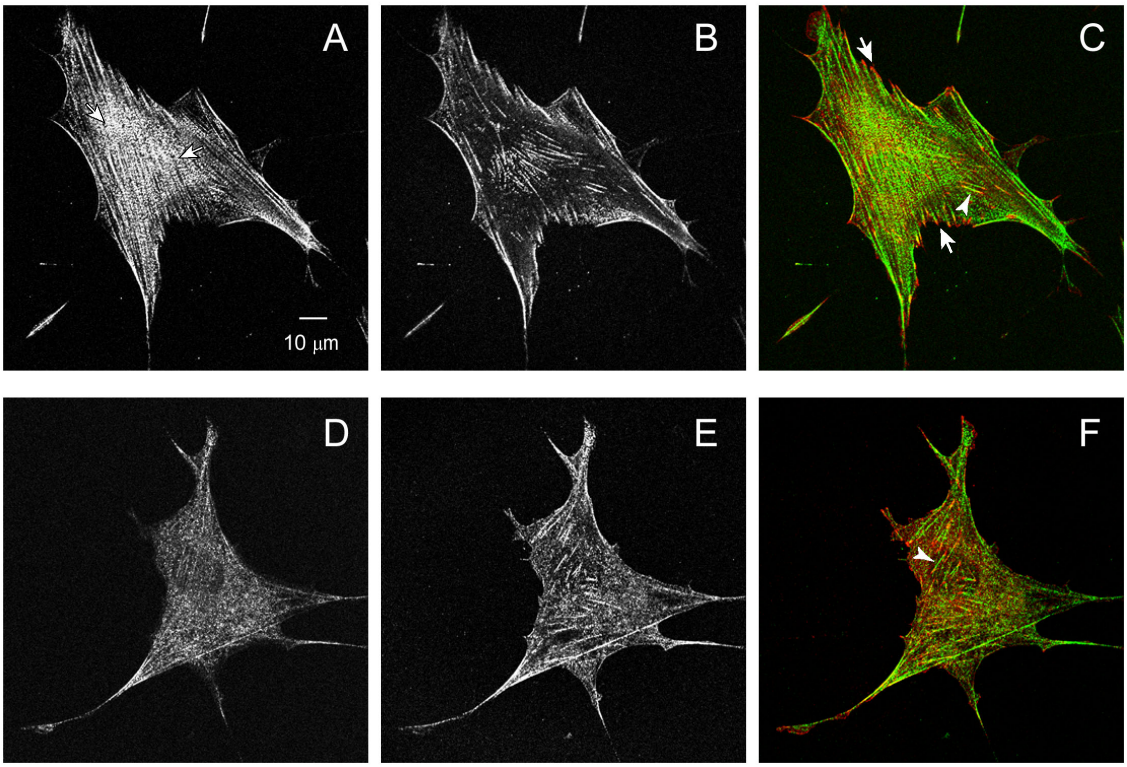

Fig. 5.